A universal scaling of planar fault energy barriers in face-centered cubic metals

Z-H. Jin[a,b]*, S. T. Dunham[c], H. Gleiter[b], H. Hahn[b], P. Gumbsch[d,e],

[a]School of Materials Science and Engineering, Shanghai Jiao Tong University, 200240 Shanghai, China

[b]Institut für Nanotechnologie (INT), Karlsruher Institut für Technologie, 76021 Karlsruhe, Germany

[c]Department of Electrical Engineering, University of Washington, Seattle, WA 98195

[d]Institut für Zuverlässigkeit von Bauteilen und Systemen (IZBS), Karlsruher Institut für Technologie, 76131 Karlsruhe, Germany

[e]Fraunhofer Institut für Werkstoffmechanik (IWM), 79108 Freiburg, Germany

*Corresponding author. Tel/fax.: +86 21 54745427; e-mail: jinzh@sjtu.edu.cn

Abstract

Minimum energy paths for generating intrinsic, extrinsic and twin planar faults were calculated for a number of face-centered cubic (fcc) metals via ab initio techniques. It is found that when the lattice is faulted sequentially, the interaction with the existing fault tends to remain minimal for nearly all the fcc metals. Accordingly, a universal scaling law may be deduced based on a single parameter – the ratio between the intrinsic stacking fault energy and the relevant energy barrier.

Keywords: metal and alloys; generalized stacking fault energies; lattice dislocation and planar fault; twinning; first-principle calculation

The plastic deformation of crystalline ductile materials at low temperatures is mediated by dislocation slip as well as mechanical twinning [1-3]. In comparison to coarse-grained polycrystalline materials, an enhanced dislocation density due to emission of partial dislocations, perfect dislocations and microtwins from grain boundary sources have been reported in several nanostructured fcc metals [4-9]. The underlying fundamental processes and defect structures are not yet fully understood. For example, in materials with high energies of intrinsic stacking faults (ISF) and high coherent twin boundary energies such as Al, twinning is believed to be difficult. Nevertheless, atomistic simulations and experimental observations suggest twinning to occur readily in Al [4,5]. On the other hand, recent experiments indicate that the yield strength as well as ductility can be enhanced in materials with low ISF-energies such as Cu [10-13] and stainless steels [14] due to preexisting nanoscale twins. However, similar effects do not seem to exist in Al [15-19].

Energies of planar faults are fundamental properties underlying mechanical deformation, solid-state phase transformation and diffusion of alloying elements in materials of different crystalline structures [1-3]. The minimum energy barrier, namely, the unstable fault energy, provides an essential measure to produce a stable fault within a perfect lattice [20-22]. Both stable and unstable fault energies can be calculated according to the minimum energy pathway along a fault plane, also known as the generalized stacking-fault (GSF) energy curve or γ-surfaces. Although GSF energies for fcc metals and alloys have been well-studied recently via various computational approaches [23-34], it remains unclear how planar faults multiply and interact with existing faults in different materials.

In this paper, energies associated with intrinsic stacking faults, ISF, extrinsic stacking faults, ESF, and twin faults, TF, in fcc lattice are calculated to elucidate correlations among stable and unstable fault energies. To clarify the general material dependence, we shall try to deduce a universal scaling law based on a single parameter, Λ, the ratio between the ISF-energy and the unstable

stacking fault energy associated with an ISF. In order to do so, the minimum energy barriers of following paths were calculated (see Fig. 1, for Al, Cu and Pt):

γ(perfect lattice → ISF) – the energy path of a crystal when it transformed from a perfect fcc lattice into an ISF of energy γ_{isf}. The saddle point of the transition defines the unstable stacking fault energy, γ_{usf} (Fig. 1, diagram on the left side).

γ(ISF → ESF) – the energy path of a crystal when it transforms from an ISF into an ESFof energy γ_{esf}. The saddle point of the transition defines the unstable energy, γ_{utf}^{1} (Fig. 1, diagram in the middle).

γ(TF → TF□)– the energy path for twinning based on a single twin boundary or a twin fault (TF) of energy γ_{tf}. The saddle point energy defines the unstable energy for twinning, γ_{utf}^{∞} (Fig.1, diagram on the right side). An extrinsic fault may develop into two well-separated twin faults to form a thick twin lamella in such a way.

We consider all the common fcc metals Ag, Au, Cu, Ni, Pd, Pt, Ir, Al and Pb in our calculations. The γ-surfaces were mapped out via fully converged calculations with the climbing-image nudged elastic band (ciNEB) method [35] in combination with the *ab initio* density-functional theory (DFT). The NEB method [36] is an efficient path technique for finding corresponding minimum energy paths between a given initial and final state of a transition, with essentially no limitation on the degrees of freedom for atomic/ionic relaxations.

DFT computations were performed using the Vienna ab initio Simulation Package (VASP) [37,38]. The full-potential projector augmented-wave method was used with core-valence electron interactions treated within the standard Blöchl scheme [39,40]. The supercell contains 12~21 $\{111\}$ layers, with a vacuum gap corresponding to 3~4 $\{111\}$ layers in the <111> direction to accommodate out-of-plane relaxations. The supercell volume and its shape were fixed during energy minimizations

of the elastic band. If the magnetism does not influence appreciably the ground energy difference between the fcc and the hcp phase, it is unlikely to change the corresponding unstable fault energies significantly. Therefore, all our calculations were done in non-magnetic state. Details for computations can be found in Table 1.

Converged minimum energy pathways were show in Fig. 1 (lower panel) for Al, Cu and Pt. All obtained stable and unstable fault energies were summarized in table 1. As may be seen in table 1, these fault energies were found to correlate according to the following linear relations:

(i) For stable faults, the energy γ_{esf} is close to γ_{isf} and nearly twice of γ_{tf}, i.e., $\gamma_{\mathrm{isf}} \simeq \gamma_{\mathrm{esf}} \simeq 2\gamma_{\mathrm{tf}}$, consistent with the well-known rule of thumb in literature [1]. It implies that both ISFs and ESFs can be thought of as one pair of TFs on neighboring planes, with energies nearly the same as for two well-separated TFs.

(ii) When a fault is produced by sliding two parts of a crystal across a single atomic plane, the transition state energy satisfy

$$\gamma_{\mathrm{usf}} \simeq \gamma_{\mathrm{utf}}^{1} - \tfrac{1}{2}\gamma_{\mathrm{isf}} \simeq \gamma_{\mathrm{utf}}^{\infty} \qquad (1)$$

This relation implies that the resisting force of the lattice neither changes significantly from one pathway to another, nor is it altered by an existing fault. In other words, when the lattice is faulted sequentially, Eq. 1 holds as long as the interaction with existing fault remains minimal. It applies for nearly all metals we considered so far except for Pt which shows reduced energy barriers along both ESF and TF pathways (Fig. 1).

Based on these observations, the ratio $\Lambda \equiv \gamma_{\mathrm{isf}} / \gamma_{\mathrm{usf}}$ (see table 1) can be used as a characteristic material measure by which a scaling law can be deduced according to Eq. 1

$$\gamma_{\mathrm{utf}}^{1} / \gamma_{\mathrm{usf}} \simeq \Lambda/2 + 1 \qquad (2)$$

As can be seen in Fig. 2, the plot reveals that, from Ag to Pb, our data scales remarkably well according to the linear relation, Eq. 2. The Lennard-Jones (LJ) system has been included as a limiting case on the left hand side because for this well-studied model material the stacking fault and twin fault energies are nearly zero, with $\Lambda \simeq 0$ and $\gamma_{\mathrm{utf}}^{1} / \gamma_{\mathrm{usf}} \simeq 1$. On the right hand side, Al ($\Lambda \simeq 0.8$) and Pb ($\Lambda \simeq 0.88$) are found to locate quite close to the other limiting case, a fcc material with Λ=1 and $\gamma_{\mathrm{utf}}^{1} / \gamma_{\mathrm{usf}}$ =3/2. For Pt the value of Λ is found to be exactly unity, however, the $\gamma_{\mathrm{utf}}^{1} / \gamma_{\mathrm{usf}}$ ratio for Pt turns out to be merely 1.07, far from expected. To understand why Eq. 1 applies to other metals but not to Pt, we examined both ionic displacements and charge distributions when the lattice is faulted.

For metals with large Λ values, charge density plots reveal that γ-surfaces are dominated by directional bonds associated with *s-p* band for the simple metals such as for Al and Pb or partially filled *d*-band for transition metals such as Ni, Pd, Ir and Pt. When two parts of a crystal are displaced relative to each other, the bonds retreat locally to resist shear (see e.g. Fig. 3a for Al). The reduced bonding gives rise to the energy of the γ-surface. If the change in bonding characteristic is confined within two adjacent planes, the energy barrier remains unaltered from one path to another (Eq. 1 and Fig. 1). This justifies that γ_{usf}, together with γ_{isf}, may define a characteristic material measure (Λ) such that Eq. 2 applies.

As shown in Fig. 3a, to generate a fault in Al, only ions belonging to the two adjacent {111} fault planes undergo large strains and significant charge redistributions. That is, as a fault (e.g. ESF or TF) is generated based on an existing fault (e.g. ISF) a minimum interaction with the existing fault is maintained due to the lattice rigidity.

This does not apply for Pt. In the case of Pt, the electronic structure is changed significantly in at least two {111} atomic planes. Several atomic planes are therefore involved and couple strongly as a new fault is generated (Fig. 3b). As can be seen in Fig. 3b, together with the change of bonding

characteristic, atoms in several adjacent {111} lattice planes are displaced due to strong interactions between the existing fault and the newly generated fault.

The linear scaling shown in Fig. 2 is also supported by results in several previous publications [25-32]. Data obtained recently for a number of fcc elements via Naval Research Lab Tight-Binding (NRLTB) codes [26,27] have been depicted in the same plot. They scale equally well and obey the same trend despite the fact that the calculated Λ's for the same element depend on the particular set of tight-binding parameters. While stacking fault energies of alloy systems may depend strongly on alloying elements and concentrations, we found that Eq. 2 still applies for Cu-Al alloys [32] (Fig. 2).

For metals of low-Λ, such as Cu with a filled *d*-band, the bonding can be mapped quite well on central-force type atomic interactions. The scaling law revealed by Eq. 2 in general applies. In some cases, central-force interatomic potentials underestimate the ratio $\gamma_{\mathrm{utf}}^{1}/\gamma_{\mathrm{usf}}$ although the ratio Λ may be reproduced reasonably well [26,28]. The scaling law (Eq. 2) therefore constitutes a useful guidance for fitting empirical interatomic interactions [41].

A more generalized version of Eq. 2 can be written as $\gamma_{\mathrm{utf}}^{1}/\gamma_{\mathrm{usf}} \simeq \Lambda/2+\beta_1$. The minimum interaction principle satisfies if $\beta_1 \simeq 1$ (see table 1) and the planar fault configuration in this case is characterized by localized bonding effects. We found that for hcp metals such as Mg, the same scaling rule ($\beta_1 \simeq 1$) is obeyed when faults are generated sequentially along basal planes [42].

In nanosctructured fcc metals, the trend to emit partial dislocation, perfect dislocation and twin can be understood in terms of the energy barriers on γ-surfaces. For large values of Λ (e.g., Al), emission of trailing partials leading to perfect dislocations is generally favored over twin nucleation ($\gamma_{\mathrm{usf}}-\gamma_{\mathrm{isf}}$ vs. $\gamma_{\mathrm{utf}}^{1}-\gamma_{\mathrm{isf}}$), but once nucleated twins can grow readily ($\gamma_{\mathrm{utf}}^{\infty}-\gamma_{\mathrm{tf}}$ vs. γ_{usf}) [4,15-18]. For small values of Λ (e.g., Cu), there is little difference in the barriers associated with twin growth and the emission of independent leading partials, so the latter is likely to dominate the response to

deformation and the strengthening role due to existing twins can be expected to be most significant [10-16].

The scaling law of Eq. 2 comprises a broad range of fcc materials. If Eq. 2 holds, it can be readily applied to reveal a general trend of mechanical twinning for fcc metals. Based on mechanical analyses of dislocation versus twin emission from a crack-tip [43], a dimensionless measure, the so-called 'twinnability', was introduced by Tadmor and Hai [44] as an intrinsic material property. Asaro and Suresh [45] proposed that in nanostructured fcc materials, the situation of dislocation vs. microtwin emission from grain boundary sources is similar to that from a crack-tip. They considered the most favorable geometry condition for twinning and derived a modified twinnability measure

$$T = \sqrt{\left(3\gamma_{\mathrm{usf}} - 2\gamma_{\mathrm{isf}}\right)/\gamma_{\mathrm{utf}}^{1}} \qquad (3)$$

The twinability T offers a mechanical criterion: if T>1, twin emission is favored over the emission of a trailing partial dislocation and thus of the emission of a perfect dislocation. Using the single ratio Λ and our scaling law, T can be converted into

$$T \simeq \sqrt{\left(3-2\Lambda\right)/\left(1+\Lambda/2\right)} \qquad (4)$$

Using the same set of data as in Fig. 2a, the computed twinability T according to Eq. 3 is plotted in Fig. 2b together with the scaling trend based on Eq. 4. It is evident that to evaluate the trend of twin emission for different fcc materials, one has to consider Λ instead of the ISF energy alone.

Eq. 4 suggests that in general twinning should be prohibited in nanostructured metals with Λ>0.8. Otherwise, twinning constitutes a competitive mode of deformation along with dislocation mediated slip. This is in agreement with experimental observations of twinning in metals such as Cu, Ni and Pd [7-9]. In the plot, Al represents a marginal case for allowing twin emission, which is also consistent with the experimental conclusion that twinning rarely occurs for this metal [18]. However, it has been argued that in nanoscale domain, small grain size increases the partial dislocation

separation distance, aiding twinning [7]. For Pt, twin emission is most difficult according to our results as well as NRLTB calculations [26,27]. Since the twinnability measure given by Eqs. 3 and 4 relies on the assumption that microtwin emission from grain boundary sources is similar to that from a crack-tip, it may fail if deformation twinning occurs via different mechanisms [46-50].

Acknowledgements

We thank M. Hettler for technical supports on parallel computations. STD acknowledges supports from Forschungszentrum Karlsruhe and the Center for Functional Nanostructures, Universität Karlsruhe (TH). This work was funded by the Deutsche Forschungsgemeinschaft (DFG) and the National Natural Science Foundation of China (Grant Nos. 50890174 & 50971088).

References

[1] J.P. Hirth, J. Lothe, Theory of Dislocations, Wiley, New York, 1982.

[2] J.A. Venables, Philos. Mag. 6 (1961) 379.

[3] J.W. Christian, S. Mahajan, Prog. Mater Sci 39 (1995) 1.

[4] V. Yamakov, D. Wolf, S.R. Phillpot, A.K. Mukherjee, H. Gleiter, Nat. Mater. 1 (2002) 45.

[5] M.W. Chen, E. Ma, K.J. Hemker, H.W. Sheng, Y.M. Wang, X.M. Cheng, Science 300 (2003) 1275.

[6] J. Schiøtz, K.W. Jacobsen, Science 301 (2003) 1357.

[7] X.Z. Liao, Y.H. Zhao, S.G. Srinivasan, Y.T. Zhu, R.Z. Valiev, D.V. Gunderov, Appl. Phys. Lett. 84 (2004) 592.

[8] H. Rösner, J. Markmann, J. Weissmüller, Philos. Mag. Lett. 84 (2004) 321.

[9] X. Wu, Y.T. Zhu, M.W. Chen, E. Ma, Scripta Mater. 54 (2006) 1685.

[10] Y.F. Shen, L. Lu, Q.H. Lu, Z.H. Jin, K. Lu, Scripta Mater. 52 (2005) 989.

[11] L. Lu, Y.F. Shen, X.H. Chen, L.H. Qian, K. Lu. Science 304 (2004) 422.

[12] L. Lu, X. Chen, X. Huang, K. Lu, Science 323 (2009) 607.

[13] L. Lu, R. Schwaiger, Z.W. Shan, M. Dao, K. Lu, S. Suresh, Acta Mater. 53 (2005) 21169.

[14] X. Zhang, A. Misra, H. Wang, M. Nastas, J.D. Embury, T.E. Mitchell, R.G. Hoagland, J.P. Hirth, Appl. Phys. Lett. 84 (2004) 1096.

[15] Z.H. Jin, P. Gumbsch, E. Ma, K. Albe, K. Lu, H. Hahn, H. Gleiter, Scripta Mater. 54 (2006) 1163.

[16] Z.H. Jin, P. Gumbsch, E. Ma, K. Albe, K. Lu, H. Gleiter, H. Hahn, Acta Mater. 56 (2008) 1126.

[17] A. Frøseth, H.V. Swygenhoven, P.M. Derlet, Acta Mater. 52 (2004) 2259.

[18] M.A. Meyers, A. Mishra, D.J. Benson, Prog. Mater. Sci. 51 (2006) 427.

[19] T. Zhu, J. Li, Prog. Mater. Sci. 55 (2010) 710.

[20] V. Vitek, Philos. Mag. 18 (1968) 773.

[21] A.T. Paxton, P. Gumbsch, M.A. Methfessel, Philos. Mag. Lett. 63 (1991) 267.

[22] D. Roundy, C.R. Krenn, M.L. Cohen, and J.W. Morris, Jr., Phys. Rev. Lett. 82 (1999) 2713.

[23] J.A. Zimmerman, H. Gao, F.F. Abraham, Model. Simul. Mater. Sc. 8 (2000) 103.

[24] G. Lu, D. Orlikowski, I. Park, O. Politano, E. Kaxiras, Phys. Rev. B 65 (2002) 064102.

[25] S. Ogata, J. Li, S. Yip, Science 298 (2002) 807.

[26] E.B. Tadmor, N. Bernstein. J. Mech. Phys. Solids 52 (2004) 2507.

[27] N. Bernstein, E.B. Tadmor, Phys. Rev. B 69 (2004) 094116.

[28] H.V. Swygenhoven, P.M. Derlet, A.G. Frøseth, Nat. Mater. 3 (2004) 399.

[29] S. Ogata,J. Li, S. Yip, Phys. Rev. B 71 (2005) 224102.

[30] D.J. Siegel, Appl. Phys. Lett. 87 (2005) 121901.

[31] D. Finkenstadt, D.D. Johnson, Phys. Rev. B 73 (2006) 024101.

[32] S. Kibey, J.B. Liu, D.D. Johnson, H. Sehitoglu, Appl. Phys. Lett. 89 (2006) 191911.

[33] M. Jahnátek, J. Hafner, M. Krajčí, Phys. Rev. B 79 (2009) 224103.

[34] Y. Wang, J. Li, Acta Mater. 58 (2010) 1212.

[35] G. Henkelman, B.P. Uberuaga, H. Jónsson, J. Chem. Phys. 113 (2000) 9901.

[36] H. Jónsson, G. Mills, K.W. Jacobsen, Nudged elastic band method for finding minimum energy paths of transitions, in: B.J. Berne, C. Ciccotti, D.F. Coker (Eds.), Classical and Quantum Dynamics in Condensed Phase Simulations, World Scientific, 1998, pp. 385-404.

[37] G. Kresse, J. Hafner, Phys. Rev. B 47 (1993) 558.

[38] G. Kresse, J. Furthmüller, Phys. Rev. B 54 (1996) 11169.

[39] P.E. Blöchl, Phys. Rev. B 50 (1994) 17953.

[40] G. Kresse, D. Joubert, Phys. Rev. B 59 (1999) 1758.

[41] Y. Mishin, M. Asta, J. Li, Acta Mater. 58 (2010) 1117.

[42] J. Han, X.M. Su, Z.H. Jin, Y.T. Zhu, manuscript submitted.

[43] J.R. Rice, J. Mech. Phys. Solids 40 (1992) 239.

[44] E.B. Tadmor, S.A. Hai, J. Mech. Phys. Solids 51 (2003) 765.

[45] R.J. Asaro, S. Suresh, Acta Mater. 53 (2005) 3369.

[46] V.R. Parameswaran, J. Weertman, J. Mater. Sci. 4 (1969) 646.

[47] E. El-Danaf, S.R. Kalidindi, R.D. Doherty, Metall. Mater. Trans. A 30 (1999) 1223.

[48] D.H. Warner, W.A. Curtin, S. Qu. Nat. Mater. 6 (2007) 876.

[49] Y.B. Wang, M.L. Sui, Mater. Sci. Forum 63 (2010) 633.

[50] Q. Yu, Z.W. Shan, J. Li, X.X. Huang, L. Xiao, J. Sun, E. Ma, Nature, 463 (2010) 335.

Table 1 Stable and unstable fault energies calculated using ciNEB-DFT methods (units in mJ/m^2). Correlation parameters, α_0, α_1 , β_1 and β_∞, are dimensionless ratios defined according to $\gamma_{\mathrm{isf}} = \alpha_0 \gamma_{\mathrm{tf}}$, $\gamma_{\mathrm{esf}} = \alpha_1 \gamma_{\mathrm{tf}}$, $\gamma^1_{\mathrm{utf}} - \frac{1}{2}\gamma_{\mathrm{isf}} = \beta_1 \gamma_{\mathrm{usf}}$ and $\gamma^\infty_{\mathrm{utf}} = \beta_\infty \gamma_{\mathrm{usf}}$, respectively. The parameters α_0, α_1 are close to 2, and β_1 and β_∞ are close to unity for all metals considered except for Pt. The ratio $\Lambda \equiv \gamma_{\mathrm{isf}} / \gamma_{\mathrm{usf}}$ has been introduced as a characteristic material measure. [Details for DFT calculations: (1) Cutoff energies (eV) for plane wave basis sets, from Ag to Pt: 337, 328, 312, 302, 253, 326, 300, 324 and 288; (2) Brillouin zone sampling was performed using the Methfessel-Paxton smearing method with the k-point meshes: 18×25×2 for Al, 12×17×2 for Ag, Cu, Au and Pb, 12×15×3 for Ni and Ir, 11×17×2 for Pd and Pt, respectively; (3) Equilibrium lattice parameter (a0, Å), from Ag to Pt : 4.166, 3.635, 4.174, 3.52, 3.86, 3.955, 4.05, 5.044 and 3.98; (4) The supercell contains 20~21 $\{111\}$ layers or 40~42 ions, except for Ni and Pd (12-layer, 24 ions).]

	γ_{isf}	γ_{esf}	γ_{tf}	γ_{usf}	γ^1_{utf}	$\gamma^\infty_{\mathrm{utf}}$	α_0	α_1	β_1	β_∞	Λ
Silver	16	12	8	91	100	93	2.08	1.56	**1.0**	1.01	**0.18**
Copper	36	40	18	158	179	161	2.0	2.22	**1.02**	1.02	**0.23**
Gold	25	27	12	68	79	72	1.98	2.16	**0.98**	1.04	**0.36**
Nickel	133	138	65	258	323	251	2.05	2.12	**0.99**	0.97	**0.52**
Iridium	334	327	160	625	818	624	2.09	2.04	**1.04**	1.0	**0.53**
Palladium	134	129	63	202	261	190	2.13	2.05	**0.96**	0.94	**0.66**
Aluminum	112	112	50	140	196	135	2.24	2.24	**1.0**	0.96	**0.80**
Lead	48	48	23	55	79	53	2.07	2.05	**1.0**	0.96	**0.88**
Platinum	286	284	137	286	305	189	2.09	2.07	**0.57**	0.66	**1.0**

Figure Captions

Fig. 1 Fault/twinning pathways by displacing the two parts of a crystal along a (111) fault plane. The displacement along each pathway is given by the Burgers vector of a Shockley partial dislocation, $\mathbf{b}_S = \frac{a_0}{6}\langle 11\bar{2}\rangle$. **Upper panel:** schematic of stacking faults formation via $\{111\}\langle 11\bar{2}\rangle$ slip in fcc metals. **Lower panel:** minimum energy pathways (γ-surfaces) for Al, Cu and Pt, obtained via converged NEB-DFT calculations. Along each path, five images were used to build the elastic band between the given initial and final state. The saddle point energy (the energy extremes) defines the unstable fault energy. The γ-surface is defined by $\gamma = (E - E_0)/A$, where E is the energy of the optimized elastic band, E_0 is the energy of the fault-free state and A is the area of the fault plane. Stable and unstable energies are marked following the pathway for Al. Vertical bars measure the relation $\gamma_{\mathrm{usf}} \simeq \gamma^{1}_{\mathrm{utf}} - \frac{1}{2}\gamma_{\mathrm{isf}} \simeq \gamma^{\infty}_{\mathrm{utf}}$, which applies to Al and Cu but not for Pt.

Fig. 2 Scaling plot of stable and unstable fault energies. Filled symbols represent our ciNEB-DFT results. Cross symbols in grey color are data obtained via NRLTB methods (non-NEB calculations) [26,27]. With increasing Λ, those elements are Ag, Pb, Cu, Pd, Au, Ir, Pb', Al, Pt, Ir' (a prime appears if a different set of tight-binding parameters was used for the same element). For Cu-Al alloys (atomic percent of Al), data were taken from Ref. 32.

Fig. 3 Charge distributions associated with forming an ESF in Al (a) and Pt (b). Vector plots at the right side represent ionic displacements between the saddle point image and its neighboring 'up-hill' image (cross symbols, cf. Fig. 1, lower panel), magnified by a factor of 2.5 (ionic positions of the initial image (ISF) and the final image (ESF) are drawn with open circles and dots, respectively; as guide for eyes, dashed and full lines are used to indicate ionic positions at different states).

Charges are depicted at an iso-surface value, 0.18 $eÅ^{-3}$ for Al and 0.23 $eÅ^{-3}$ for Pt, with ions shown by blue balls. In both metals the atomic bonds are highly directional. Like other metals, redistribution of charges in Al appears almost solely within the two adjacent fault planes, underlying that the interaction between faults tends to be minimal. In Pt, extended redistributions across about 5 (111) layers (marked by horizontal dashed lines) are observed, suggests strong coupling between faults or change of bonds involving multiple (111) layers for both stable and unstable fault configurations.

Fig. 4 The universal trend of twinning according to a twinnability measure (*T*) defined by Asaro and Suresh [45].

Figure(s)

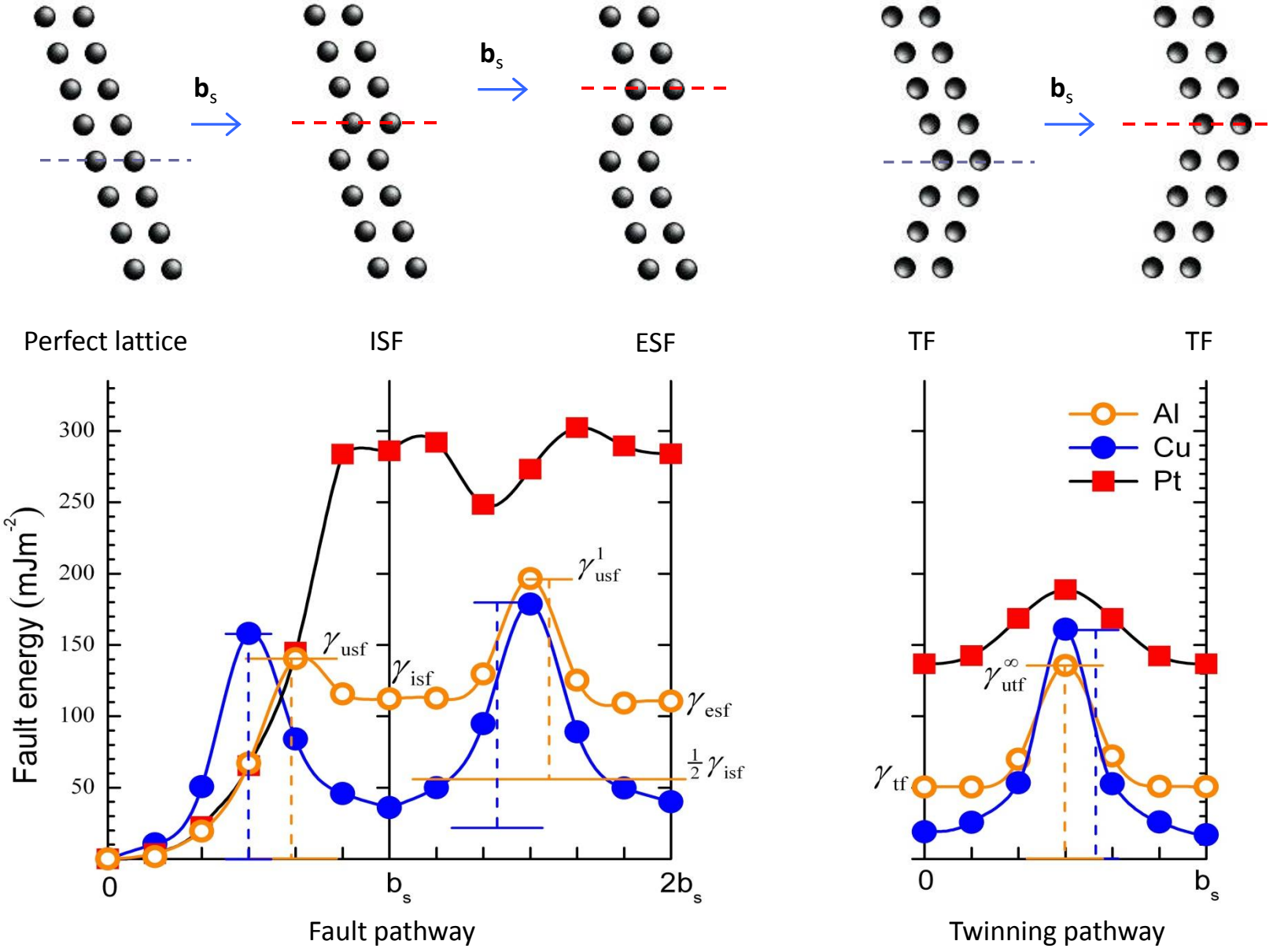

Fig. 1, Jin

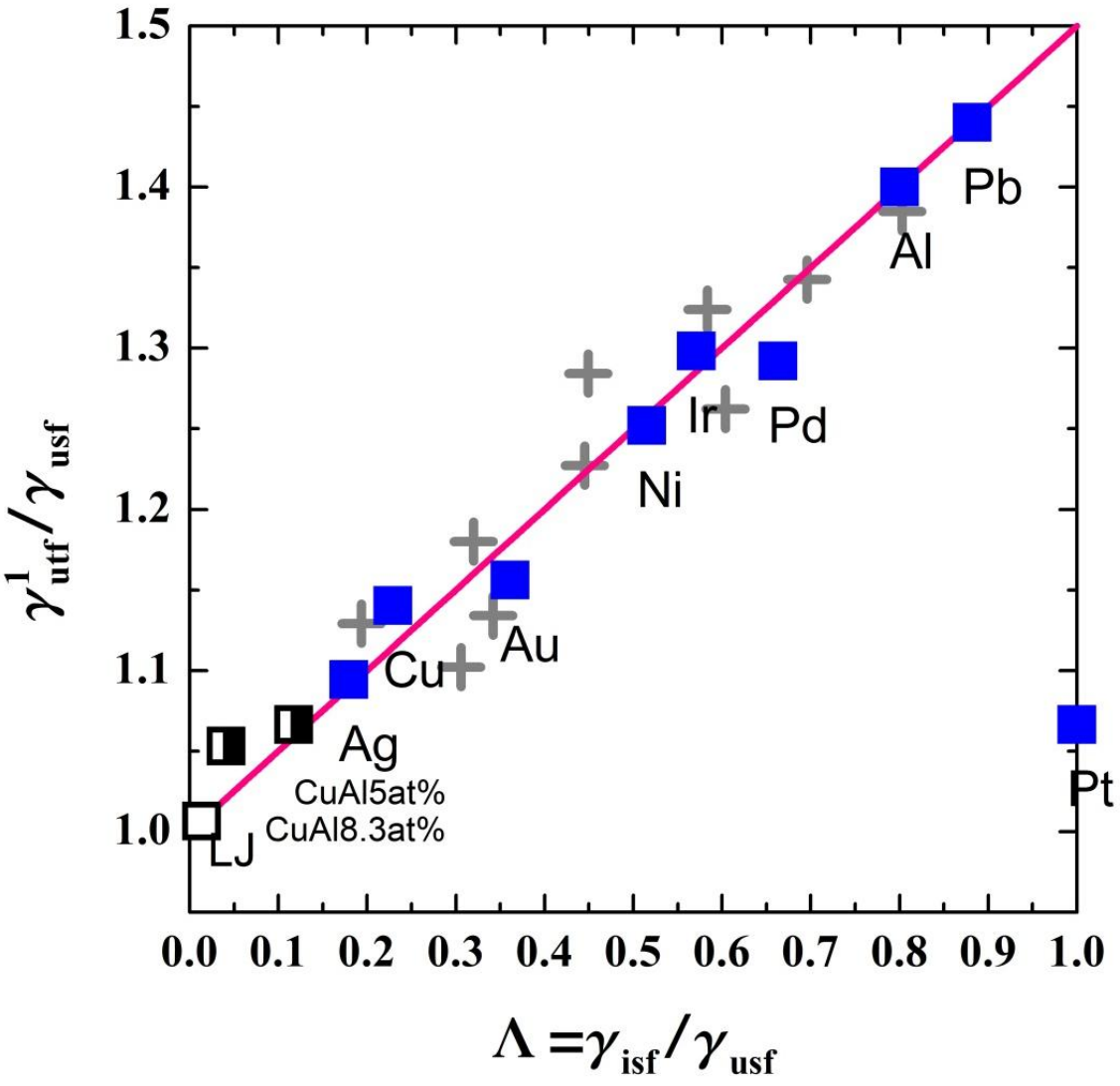
1.5
1.4
1.3
1.2
1.1
1.0
0.0 0.1 0.2 0.3 0.4 0.5 0.6 0.7 0.8 0.9 1.0
$\gamma^1_{utf}/\gamma_{usf}$
$\Lambda = \gamma_{isf}/\gamma_{usf}$
Pb
Al
Ir
Pd
Ni
Au
Cu
Ag
CuAl5at%
CuAl8.3at%
LJ
Pt

Fig. 2, Jin

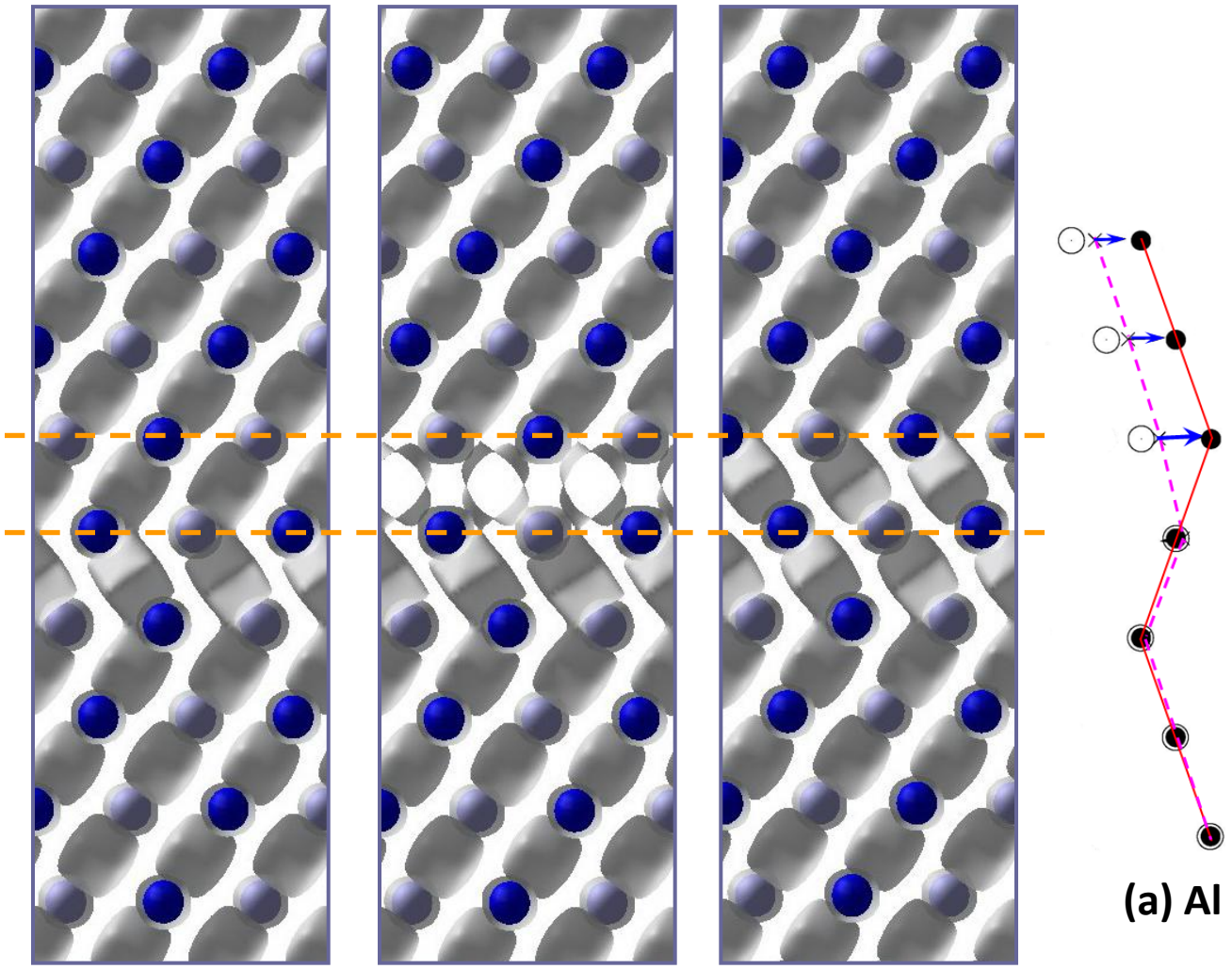

Fig. 3a, Jin

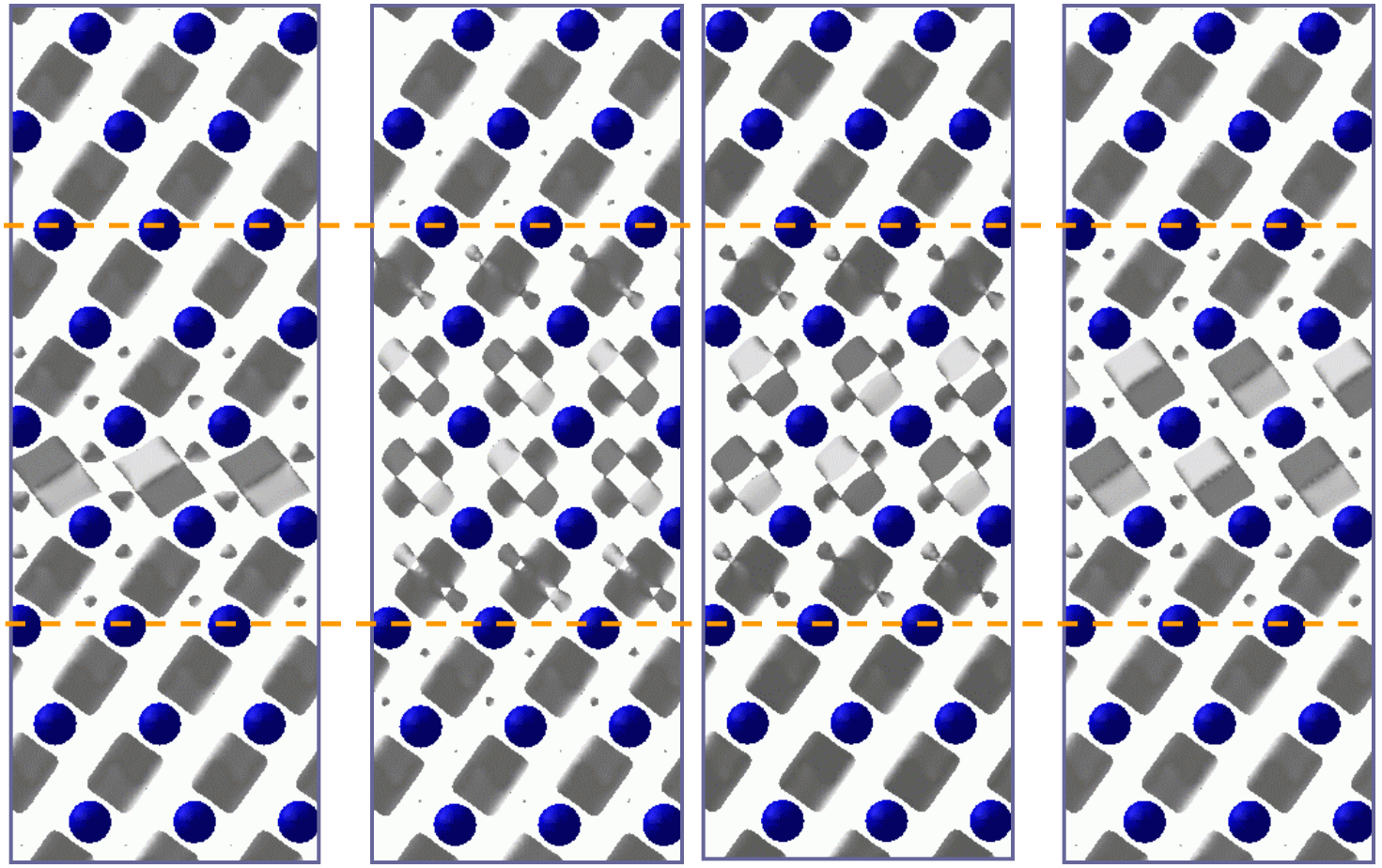

Intrinsic fault

Unstable faults

Extrinsic fault

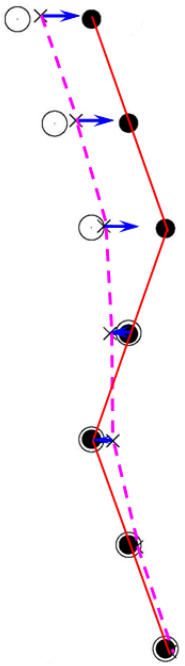

(b) Pt

Fig. 3b, Jin

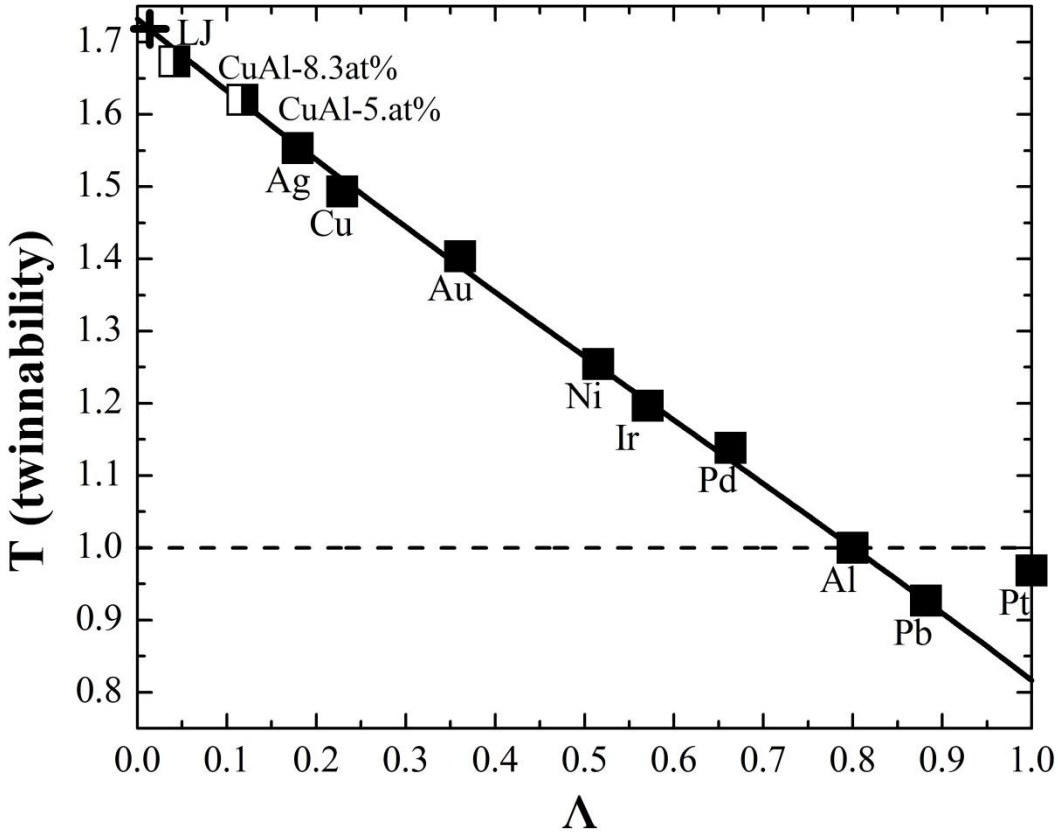
T (twinnability)
Λ
LJ
CuAl-8.3at%
CuAl-5.at%
Ag
Cu
Au
Ni
Ir
Pd
Al
Pb
Pt
1.7
1.6
1.5
1.4
1.3
1.2
1.1
1.0
0.9
0.8
0.0
0.1
0.2
0.3
0.4
0.5
0.6
0.7
0.8
0.9
1.0

Fig. 4, Jin